Integrative Biology

PAPER

The contractile strength of vascular smooth muscle myocytes is shape dependent†

Cite this: *Integr. Biol.*, 2014, 6, 152

George J. C. Ye,[a] Yvonne Aratyn-Schaus,[a] Alexander P. Nesmith,[a] Francesco S. Pasqualini,[a] Patrick W. Alford[b] and Kevin Kit Parker*[a]

Received 1st November 2013,
Accepted 21st December 2013

DOI: 10.1039/c3ib40230d

www.rsc.org/ibiology

Vascular smooth muscle cells in muscular arteries are more elongated than those in elastic arteries. Previously, we reported changes in the contractility of engineered vascular smooth muscle tissue that appeared to be correlated with the shape of the constituent cells, supporting the commonly held belief that elongated muscle geometry may allow for the better contractile tone modulation required in response to changes in blood flow and pressure. To test this hypothesis more rigorously, we developed an *in vitro* model by engineering human vascular smooth muscle cells to take on the same shapes as those seen in elastic and muscular arteries and measured their contraction during stimulation with endothelin-1. We found that in the engineered cells, actin alignment and nuclear eccentricity increased as the shape of the cell elongated. Smooth muscle cells with elongated shapes exhibited lower contractile strength but greater percentage increase in contraction after endothelin-1 stimulation. We analysed the relationship between smooth muscle contractility and subcellular architecture and found that changes in contractility were correlated with actin alignment and nuclear shape. These results suggest that elongated smooth muscle cells facilitate muscular artery tone modulation by increasing its dynamic contractile range.

Insight, innovation, integration

The shape and contractility of smooth muscle cells vary according to the type of artery, local micro-environment, developmental stage and disease. To probe the role of cell architecture in smooth muscle contractility, we engineered vascular smooth muscle cells with varying length to width ratios and measured their contractility using traction force microscopy in response to vasoactive agents. We found that while contractile strength decreased as vascular smooth muscle cell shape elongated, the dynamic range of contractility, relative to basal tone, increased with the length of the cells. These findings suggest that vascular smooth muscle cells adopt different shapes to facilitate the functions of the vasculature they constitute.

Introduction

The contractile function and structure of vascular smooth muscle cells (VSMCs) vary as a function of location in the cardiovascular system.[1] In large diameter elastic arteries, such as the aorta, VSMCs contract to maintain vessel pressure during cardiac cycle.[2] This is in contrast to mid-sized muscular arteries, such as the external carotid artery of the neck and femoral artery of the thighs, where VSM contracts concentrically to constrict or relax the arterial wall in a process called vascular tone modulation.[3] These functional differences are reflected structurally, where VSMCs exhibit markedly different geometries in these arteries. Although differentiated VSMCs in elastic and muscular arteries have a characteristic spindle shape, the elongated shape of VSMCs in muscular arteries with nearly 15 : 1 in cell length to width aspect ratio (AR), is more pronounced than those found in elastic arteries, which have cell AR about 9 : 1.[1] It has been speculated that the VSMC shape may facilitate vascular tone modulation in muscular arteries by providing better dynamic response to blood flow[4] and pressure changes.[5] However, definitive evidence to support this relationship between VSMC shape and contractile function has been limited.

VSMCs undergo significant changes in geometry in physiological and pathological developments. Domenga and colleagues demonstrated rapid VSMC structural changes in wild-type

[a] *Disease Biophysics Group, Wyss Institute for Biologically Inspired Engineering and the School of Engineering and Applied Sciences, Harvard University, 29 Oxford St, Pierce Hall 321, Cambridge, MA 02138, USA. E-mail: kkparker@seas.harvard.edu; Fax: +1-617-496-1793; Tel: +1-617-495-2850*

[b] *Department of Biomedical Engineering, University of Minnesota-Twin Cities, Minneapolis, MN 55455, USA*

† Electronic supplementary information (ESI) available. See DOI: 10.1039/c3ib40230d

mice, where VSMCs developed more elongated shape, increased thickness and become circumferentially oriented around the lumen by postnatal day 28 compared to immature VSMCs at birth.[6] Genetic deletion of *Notch3*, which is uniquely expressed in arteries but not of veins, led to thin, irregular, roundly shaped VSMCs that are poorly orientated around the lumen.[6] In human, *Notch3* mutation leads to a hereditary vascular dementia called cerebral autosomal dominant arteriopathy with subcortical infarcts and leukoencephalopathy (CADASIL), characterised by a cerebral non-atherosclerotic, non-amyloid angiopathy that mainly affects the small arteries penetrating the white matter. Patients diagnosed with this disease were usually found with more rounded and irregular VSMC shape in small- and mid-sized arteries.[7] During normal vascular repair following injury, VSMCs switch their contractile phenotype to synthetic phenotype and in the process, changing their shape from the elongated spindle morphology to an epithelioid or rhomboid morphology.[8] The epithelioid shaped VSMCs proliferate and produce extracellular matrix (ECM) to help with the wound healing process.[8] However, the deregulation of this phenotype switching process underlies a number of vascular disorders such as hypertension,[9] restenosis,[10] and vasospasm.[11] This is supported by pathological studies that observed morphologically distinct VSMC populations between spindle and epithelioid shapes at the site of atherosclerotic intima in the aorta,[12] carotid artery[13] and coronary artery.[14] Understanding the role of VSMC shape change may elucidate mechanistic insight in the context of cellular physiology and vascular pathology.

In addition to VSMCs, shape change also plays an important role in regulating the physiological and pathological development of other smooth muscle cells and cardiomyocytes. In an early ultra-structural study focusing on the prenatal development of smooth muscle in the human fetal uteri between 12–40 weeks of gestation, Konishi *et al.* showed immature uterine SMCs changed from a rounded morphology at week 12–16 to an elongated shape with identifiable dense bodies at week 18.[15] A clinical and pathological analysis of 26 cases of atypical smooth muscle tumours of the uterus demonstrated that SMC in leiomyoma changed from the typical elongated shape to a rounded, polygonal shape.[16] In cardiac development, cardiac looping is one of the first steps of forming a four chambered-heart that requires bending and twisting of heart tube asymmetrically. It was found that myocardium on the concave side of the heart tube remains thick and columnar while the convex side flattened and increased in surface area, effectively reducing the AR of the myocardium epithelial tissue[17] and resulting in different contractility on the concave and convex surfaces.[18] In mature adult heart under pathological chronic pressure overload, the heart undergoes concentric hypertrophy, resulting myocytes increase cell width without significant changes in cell length. This, in turn, decreases the normal AR from 7 : 1,[19] as seen for normal ventricular myocytes, to 5 : 1.[20] As heart continues to fail, eccentric hypertrophy develops in response to volume overload, which adds sarcomere in series without changing myocytes' cross-sectional area. This eventually increased the myocytes aspect ratio to 11 : 1.[19b,c] Investigating the shape and contractility relationship in myocytes, our group recently reported that myocytes contractility is optimised at AR observed in normal hearts and decreased in cardiomyocytes that resemble AR of failing hearts.[21] In addition, we observed that boundary condition encoded in the extracellular space can regulate myocyte tissue cytoskeletal alignment and function.[22] These studies clearly demonstrated that shape adaptations in smooth and striated muscles can profoundly influence the cellular function.

We hypothesised that forcing VSMCs to assume increasingly elongated shapes would mimic the VSMC morphology in muscular arteries *in vivo* and induce changes in the intracellular architecture that consequently increase the dynamic contractile range of VSMC in response to contractile stimuli. To test this hypothesis, we engineered VSMCs on micropatterned islands of fibronectin (FN) with ARs of 5 : 1, 10 : 1 or 20 : 1 to mimic VSMC shapes found in elastic and muscular arteries *in vivo*, quantified cytoskeletal and nuclear organization, and directly measured contraction *via* traction force microscopy (TFM) upon stimulation with the vasoconstrictor endothelin-1 (ET-1). We found that cell shape significantly influenced cytoskeletal and nuclear organization and isolated VSMCs of AR near 20 : 1 achieved lower basal and stimulated contractile forces but greater percent change in contractile force after stimulation. These results suggest that the elongated shape equips VSMC with a greater dynamic contractile range, facilitating modulation of vascular tone over a broad range by muscular arteries *in vivo*.

Results

Engineering cell shape on soft substrate

In vitro studies have revealed the unique sensitivity of VSM to the cellular micro-environment. These studies suggest that VSMC are influenced by substrate stiffness,[23] growth factor stimulation,[24] extracellular matrix (ECM) composition,[25] and geometric constraints.[26] We measured the cell spreading area of isolated VSMCs cultured on polyacrylamide (PAA) gels (Fig. 1A, inset) uniformly coated with fibronectin (FN) and found that cell spreading area is normally distributed with a mean at 4000 μm^2 (Fig. 1A). Based on 9 : 1 to 15 : 1 VSMC ARs in elastic and muscular arteries from prior *in vivo*[1] study, we selected length to width ARs of 5 : 1 (141 $\mu m \times 28 \mu m$), 10 : 1 (200 $\mu m \times 20 \mu m$) and 20 : 1 (282 $\mu m \times 14 \mu m$) as the shape of our engineered VSMCs. Utilizing a microcontact printing strategy established in our group,[21,27] we micropatterned rectangular FN islands with 5 : 1, 10 : 1 and 20 : 1 ARs on 13 kPa PAA gel surfaces (Fig. 1B). We immunostained the FN islands with anti-human FN and found them to be highly uniform (Fig. 1C). After culturing VSMCs for 72 hours on the patterned PAA substrate, isolated VSMCs with AR of 5 : 1, 10 : 1 and 20 : 1 assumed the rectangular shape of the patterned FN islands (Fig. 1D). Micropatterned VSMC thickness was measured by imaging the phalloidin stained F-actin *via* confocal

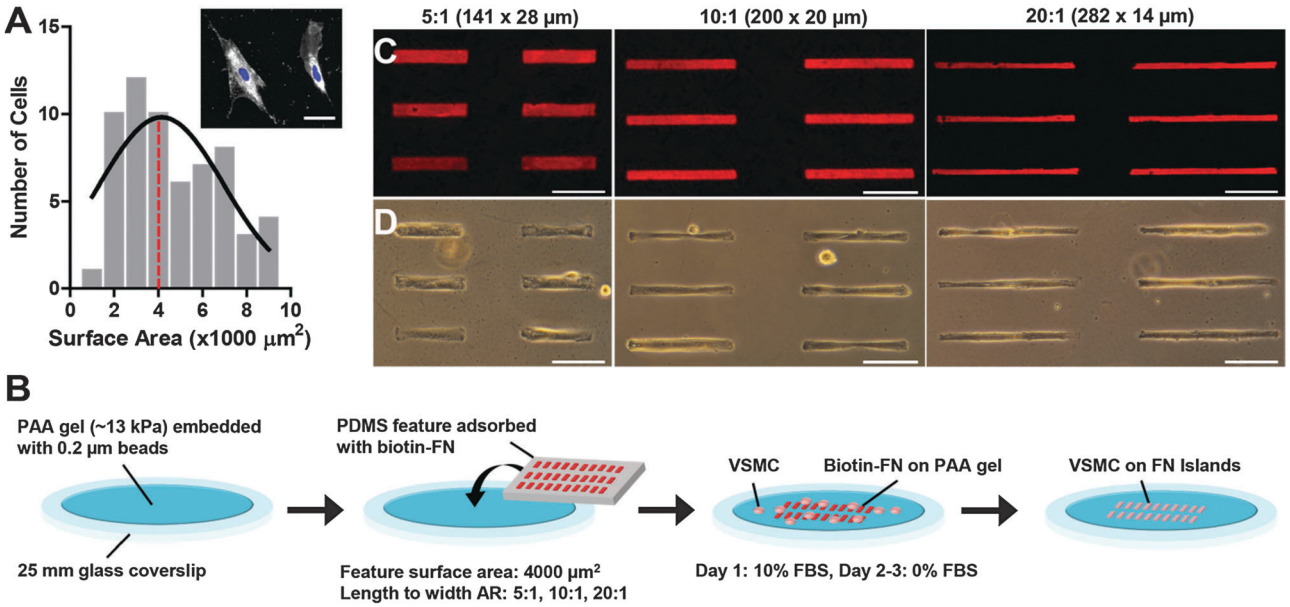

Fig. 1 Microcontact printing (μCP) of biotinylated fibronectin (biotin-FN) provided spatial cue for building isolated vascular smooth muscle cells (VSMCs). (A) VSMC surface area is normally distributed (solid line) with mean surface area of 4000 μm² (red dotted line). Inset: we labelled the cells with a lipophilic, fluorescent cell membrane stain, DiO, and DNA-binding fluorescent stain, DAPI to observe the cell membrane and nucleus, respectively. Representative DiO and DAPI stained VSMCs sparsely seeded on polyacrylamide (PAA) gel with isotropic biotin-FN are shown. (White: cell membrane, blue: nuclei). Scale bar = 50 μm. (B) Schematic representation of μCP method on PAA gel to construct isolated VSMCs with different aspect ratios (AR). (C) Anti-human FN staining of patterned biotin-FN on PAA gel. (D) Phase contract images of micropatterned isolated VSMCs with AR of 5 : 1, 10 : 1 and 20 : 1 and surface area of 4000 μm². (C and D) scale bar = 100 μm.

microscopy (Fig. S1A, ESI†). No statistically significant difference in cell thickness was observed between the three ARs, suggesting the cell volume was conserved (Fig. S1B, ESI†). Taken together this approach enabled us to engineer isolated VSMCs with cell ARs that mimic *in vivo* VSMC shape on PAA soft substrate *in vitro*.

Cytoskeletal architecture varies as a function of cell shape

Mechanical stimuli within the cellular microenvironment induce remodeling of cellular structure.[23,28] Previously, we reported distinctions in cell shape, cytoskeletal alignment, and nuclear shape in engineered vascular tissues assembled on matrix templates with varying geometries.[26a] In our engineered cells, we measured the alignment of F-actin (Fig. 2A–C, 5 : 1, 10 : 1 and 20 : 1 respectively) and nuclei, projected nuclear area and eccentricity (Fig. 2D–F, 5 : 1, 10 : 1, and 20 : 1 respectively), using fluorescent staining. The orientation of the F-actin was calculated based on a structure tensor method previously developed[29] and the global degree of cytoskeletal alignment was quantified with the orientational order parameter (OOP),[30] an indicator that ranges from a value of one for perfectly aligned samples to zero for completely random ones. The OOP is extensively used in crystallography[31] and previously used by our group for analysing the cytoskeletal organization of cardiac,[32] vascular[26a] and valve[33] cells, as well as a design parameter for the development of a biohybrid jellyfish.[34] We found that F-actin OOP increased significantly as cell AR increased (Fig. 2G), suggesting that as the cell's long axis was extended, the transverse boundary conditions on the cell potentiated the alignment of polymerizing actin with the cell's long axis.

The cell nucleus interacts with the cytoskeleton[35] and deforms when extracellular stresses are applied.[36] Changes in nuclear shape have been proposed to cause conformational changes in chromatin structure and subsequently influence transcription level and cell function.[37] We observed a marked difference in nuclear angle offset, projected area and eccentricity (Fig. 2H). Nuclear angle offset, which measures the difference in orientation between the major axes of the ellipse that best fits the cell body and nucleus (Fig. 2D), was significantly lower for cells with 20 : 1 AR (Fig. 2G). The projected nuclear area in these cells was found to decrease significantly for cells with 10 : 1 and 20 : 1 ARs (Fig. 2I). Consistent with previous findings,[26a] nuclear eccentricity significantly increased as cell AR increased (Fig. 2I). We asked whether changes in nuclear morphology could be explained by a decrease in nuclear volume resulting from cell lengthening as seen in endothelial cells.[38] Based on three-dimensional rendering of the nucleus (Fig. S2A, ESI†), we fitted it with an ellipsoid morphology[38] (Fig. S2B, ESI†) and evaluated the length, width and height of the ellipsoid (Fig. S2C, ESI†). We found that the nuclear volume and nuclear surface area were similar for all ARs with means at 475 μm³ and 464 μm² respectively (Fig. S2D, ESI†). These data suggested that VSMC shape can regulate cytoskeletal architecture by remodelling F-actin stress fibre orientation and nuclear morphology.

Elongated VSMCs exhibited greater contractile range

The primary function of VSMCs in muscular arteries is tone modulation in response to systemic and local signals to

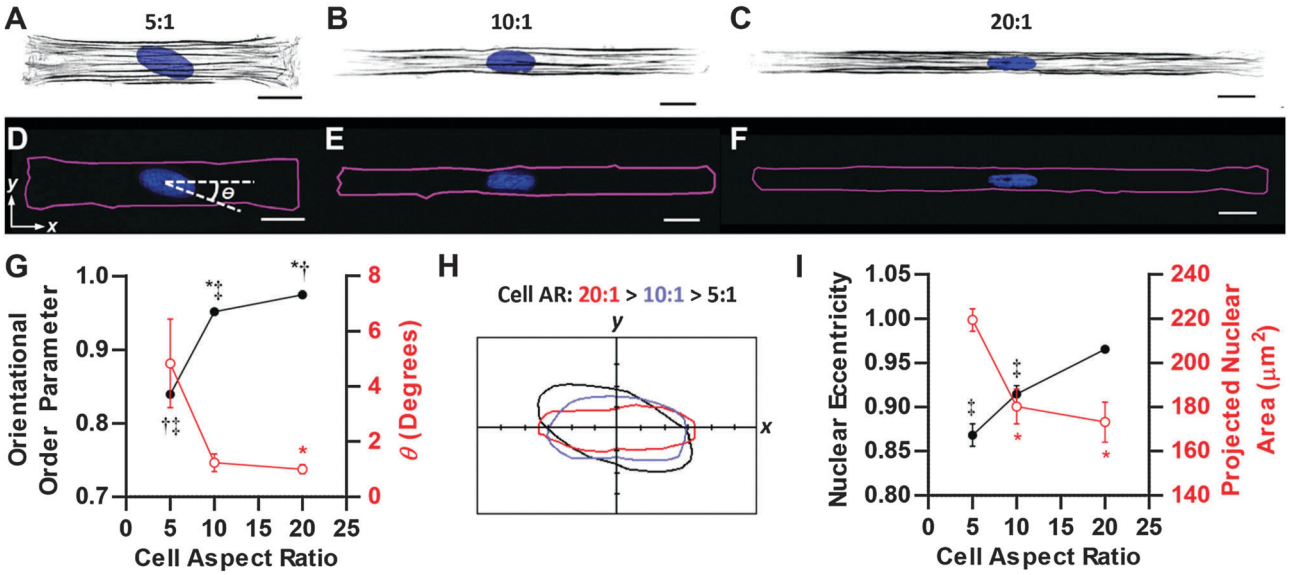

Fig. 2 AR of isolated VSMCs influences its cytoskeletal organization and nuclear morphology. (A–C) Phalloidin and DAPI stained patterned isolated VSMCs with AR of 5 : 1 (A), 10 : 1 (B) and 20 : 1 (C). (White: F-actin, blue: nuclei). Scale bar = 20 μm. (D–F) Manual traces of cell border with nuclei of isolated VSMCs in (A–C). (Magenta: cell border, blue: nuclei). Nuclear angle, θ, is shown between the two dotted white lines in (D), representing the major axes of the ellipses that best fit the cell body and nucleus respectively. Scale bar = 20 μm. (G) F-actin orientational order parameter (black) and nuclear angle offset (red) as a function of VSMC ARs. (H) Superimposed nuclear outlines from cells in D–F show clearly the differences in nuclear eccentricity, angle offset and projected area as cell AR changes. (I) Nuclear eccentricity (black) and projected area (red) as a function of VSMC ARs. * = statistically different from 5 : 1 AR, † = statically different from 10 : 1 AR, ‡ = statistically different from 20 : 1 AR. $p < 0.05$. (G, I) mean ± SEM. n = 7–12 cells per AR.

contract or relax the vessel wall.[39] We hypothesised that in our *in vitro* system, the elongated VSMC shape would improve its dynamic contractile range in response to an external stimulus. To test this hypothesis, we developed a traction force microscopy (TFM) protocol to measure contractile strength of isolated VSMCs with varying ARs prior to and after stimulation with the vasoconstrictor ET-1 (Fig. 3A). Prior to stimulation, we imaged the basal tone of isolated VSMCs. At 8 min, we stimulated contraction of the isolated VSMCs with a 100 nM dosage of ET-1. At 31 min, we treated cells with a rho-associated kinase inhibitor, HA-1077, at a saturating dosage of 100 μM to induce relaxation of the cells as previously reported by our group.[26a] Finally at 60 min, we terminated the experiment by exposing the cells to trypsin, such that there was no traction on the substrate in order to establish a reference for calculation of the absolute bead displacements. For each condition, three

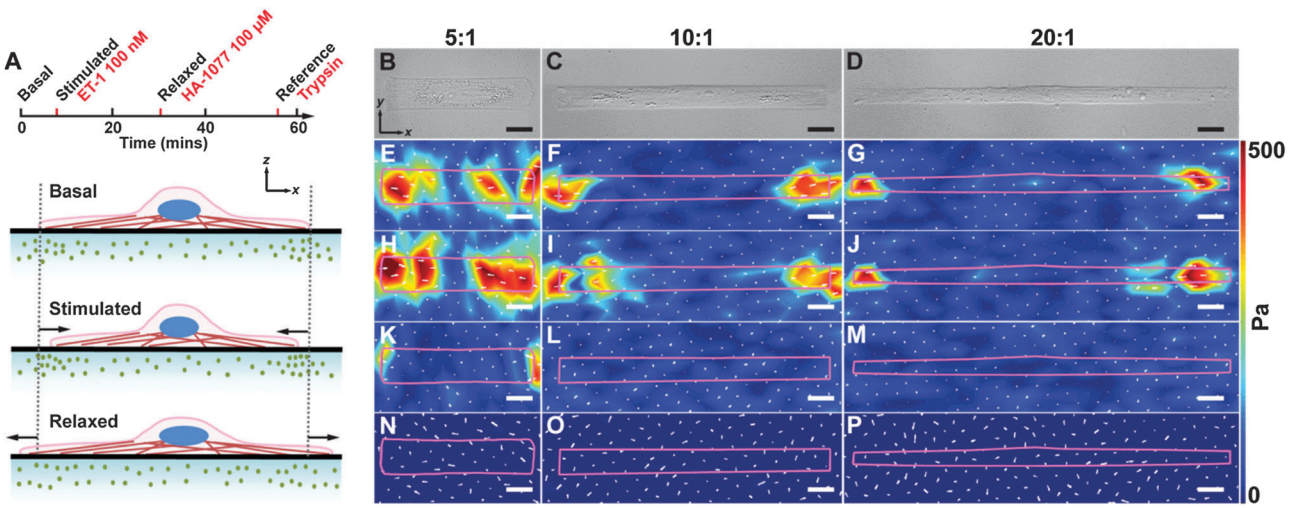

Fig. 3 Traction force microscopy experimental protocol and representative stress spatial maps of isolated VSMCs. (A) Drug administration timeline of TFM experiment for isolated VSMCs and corresponding schematic representations of cell–substrate interaction at different stages. DIC images of isolated VSMC of AR 5 : 1 (B), 10 : 1 (C) and 20 : 1 (D) and corresponding traction stress maps at basal (E–G), after stimulation with 100 nM endothelial-1 (H–J), after treatment with 100 μM HA-1077 (K–M) and finally detached with 0.5% trypsin (N–P). The longitudinal and transverse directions of the cell are defined in x- and y-axis in (B). E–P has the same colour scale to the right side. (B–P) scale bar = 20 μm.

consecutive images separated by 4 minute intervals were taken to ensure consistency in VSMC contractile output and to minimize potential phototoxic effect of laser excitation.

Prior to stimulation, we ascertained that isolated VSMCs fully occupied the rectangular FN islands by differential interference contrast (DIC) imaging. High fidelity rectangular isolated VSMCs with AR of 5 : 1 (Fig. 3B), 10 : 1 (Fig. 3C) and 20 : 1 (Fig. 3D) were selected for TFM experiments. We defined the AR of an isolated VSMC at its basal state prior to stimulation as the cellular AR. As a convention, we further defined the longitudinal and transverse directions of isolated VSMCs as the *x*- and *y*-axes, respectively (Fig. 3B). Prior to ET-1 stimulation, basal traction stresses were observed for isolated VSMCs with AR of 5 : 1 (Fig. 3E), 10 : 1 (Fig. 3F) and 20 : 1 (Fig. 3G). Following ET-1 stimulation, traction stress intensity and area both increased for AR 5 : 1 (Fig. 3H), 10 : 1 (Fig. 3I) and 20 : 1 (Fig. 3J) isolated VSMCs. After HA-1077 treatment, traction stress was significantly reduced for isolated VSMCs with AR of 5 : 1 (Fig. 3K) and completely absent for AR of 10 : 1 (Fig. 3L) and 20 : 1 (Fig. 3M). After cells were detached by trypsin, traction stress was completely absent for all ARs (Fig. 3N–P, respectively). For all three ARs, we observed that the basal (Fig. 3E–G) and ET-1 stimulated (Fig. 3H–J) traction stresses were localised at the two ends of the cells and pointed towards the geometric centre of the cell where the nucleus is generally located. This phenomenon became more pronounced for isolated VSMCs with AR 10 : 1 (Fig. 3F and I) and 20 : 1 (Fig. 3G and J).

We quantified the contractile strength of isolated VSMCs by computing the traction force (T) and strain energy[40] (U) applied by the cell on the substrate from beads displacements at basal, stimulated, and relaxed conditions with respect to the acellular reference condition. The traction force is a vector measurement, which allowed us to probe changes in contractility along either the longitudinal (Fig. 4A) or transverse (Fig. S3A, ESI†) axis of the cell. Strain energy is a scalar measurement that integrates tractions exerted in all directions (Fig. S4A, ESI†), which enabled us to measure the overall changes in cell contraction. In response to ET-1 stimulation, the isolated VSMCs contracted, increasing the measured longitudinal traction force from the initial basal tone (T_{bx}) to a higher level, here denoted as T_{cx} (Fig. 4B). Similar increases were also observed in transverse traction force (Fig. S3B, ESI†) and strain energy (Fig. S4B, ESI†). To assess the dynamic contractile range of isolated VSMCs, we computed the relative contractile increase in longitudinal traction force (K_{Tx}, Fig. 4B), transverse traction force (K_{Ty}, Fig. S3B, ESI†) and strain energy (K_u, Fig. S4B, ESI†) by normalizing the change between the basal tone to the ET-1 stimulated tone with the basal tone. These measurements allowed us to fully characterize the absolute and relative changes in contractile strength of isolated VSMCs in response to external stimuli.

We plotted the AR of each isolated VSMC against its contractile measurements. For longitudinal traction force, we found that T_{bx} (Fig. 4C) and T_{cx} (Fig. 4D) both negatively correlated with cell AR. Similar trends were observed in strain energy as U_b (Fig. S4C, ESI†) and U_c (Fig. S4D, ESI†) decreased as cell AR increased. This suggested that the absolute contractile strength of isolated VSMCs weakens as they elongate. No correlations between cell AR and transverse traction forces was observed prior to (Fig. S3C, ESI†) or after ET-1 stimulation (Fig. S3D, ESI†), suggesting that longitudinal elongation in cell shape accounts for the observed differences in contractile output. However, the relative contractile increase in longitudinal traction force (Fig. 4E, K_{Tx}) and strain energy (Fig. S4E, K_U, ESI†) significantly increased as cell AR increased, which indicates that elongated VSMCs exhibited a greater percent change in contractile strength in relation to its basal tone after stimulation with ET-1. In the transverse direction, no correlation between cell AR and relative contractile increases (K_{Ty}) were found (Fig. S3E, ESI†). Taken together, these results suggest that cell shape elongation led to a decrease in contractile strength but an increase in the dynamic contractile range along the longitudinal cell axis.

Contractility correlated with subcellular organization

We asked whether differences observed in F-actin cytoskeletal organization would reflect the differences in contractility of the cells. To answer this question, we grouped isolated VSMCs into 5 : 1, 10 : 1 and 20 : 1 ARs and compared their actin alignments with initial basal tone (T_{bx}) and relative contractile increase (K_{Tx}). We found that as OOP increased, T_{bx} decreased while K_{Tx} increased (Fig. 5A), suggesting that more aligned F-actin fibres enable greater relative increase in force generation along the fibre direction at the expense of weakened overall force output.

A previous study demonstrated that more polarised cells have reduced Rho-dependent actomyosin contractile activity.[41] We asked if the reduction in overall force generation is a result of fewer actomyosin cross-bridge cycling activities in VSMCs with more aligned F-actin fibres. Since cross-bridge cycling directly leads to cell shortening,[42] we quantified longitudinal cell shortening (ΔL) from the changes in cell length during contraction with respect to basal and relaxed states (Fig. S5A, ESI†). We found that ΔL increased for VSMC with higher ARs (Fig. S5B, ESI†) and this increase is positively correlated with OOP values (Fig. S5C, ESI†). These results suggested that cross-bridge cycling is unlikely to be the cause for the reduction in overall force generation.

Nuclear shape and surface area is influenced by cell morphology[43] and subsequently affects other cellular functions.[38] Our recent work showed that nuclear eccentricity is positively correlated with VSM tissue contractility.[26a] We asked if nuclear shape and projected area are also suggestive of the observed differences in isolated VSMC contractility. We grouped isolated VSMCs into 5 : 1, 10 : 1 and 20 : 1 ARs and compared nuclear eccentricity and projected area with T_{bx} and K_{Tx}. Here, we found that as projected nuclear area increased, T_{bx} increased while K_{Tx} decreased significantly (Fig. 5B). However, as nuclear eccentricity increased, T_{bx} decreased while K_{Tx} decreased significantly (Fig. 5C). These data suggested the morphological changes in VSMC nucleus may be an important metric for assessing the absolute and relative contractile strength of VSMCs in response to external stimuli.

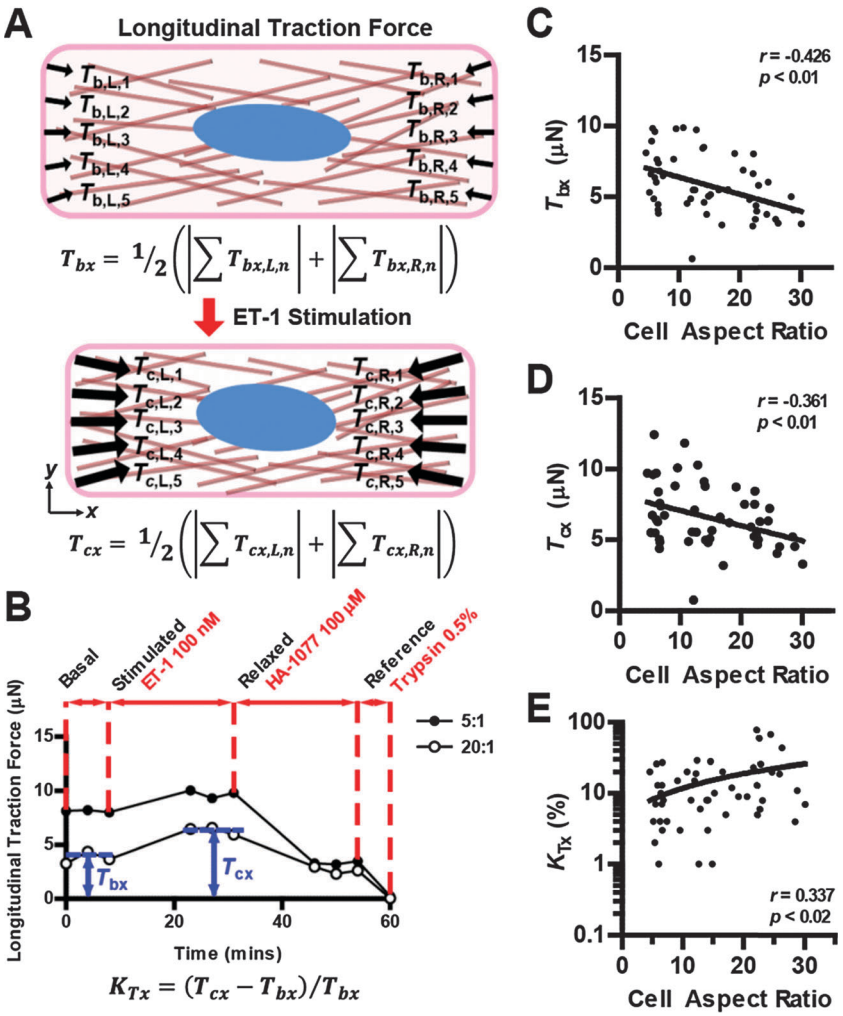

Fig. 4 Isolated VSMC AR correlated with longitudinal traction force. (A) Schematics illustrating calculations for longitudinal traction force of an isolated VSMC at basal (T_{bx}) and after stimulation with ET-1 (T_{cx}). Longitudinal traction force was calculated as half the sum of the longitudinal magnitude of all traction force vectors, assuming that each half of the cell exert an equal amount of force in opposite directions. (B) Representative temporal longitudinal traction force profiles of isolated VSMCs with AR 5 : 1 (lower bound) and 20 : 1 (upper bound) prior to and after stimulation. Relative contractile increase in longitudinal traction force (K_{Tx}) is defined as the per cent change in longitudinal traction force from basal to ET-1 stimulated. T_{bx} (C), T_{cx} (D) and K_{Tx} (E) plotted as a function of isolated VSMC ARs. (C–E) n = 14–17 cells from 4–6 experiment per AR. The correlation efficient, r, is determined by linear regression analysis. Reported p values for Pearson correlations are two-tailed, demonstrated that the correlation is significantly different from zero.

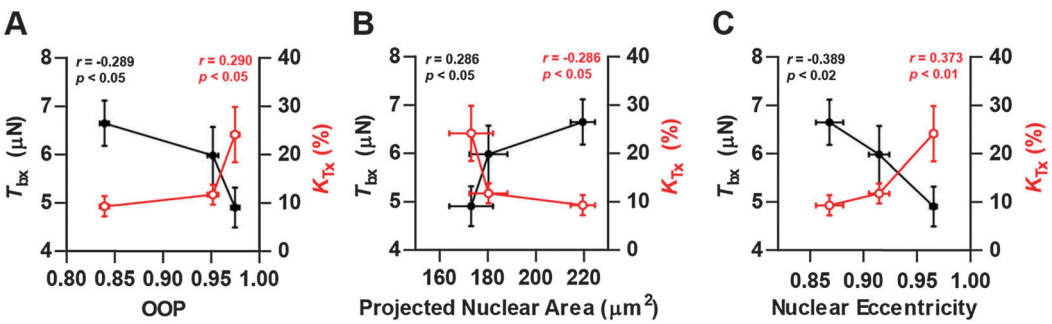

Fig. 5 Contractile output correlated with cytoskeletal organization and nuclear morphology. Basal longitudinal traction force (T_{bx}, black) and relative contractile increase (K_{Tx}, red) in longitudinal traction force after ET-1 stimulation (K_{Tx}, red) as a function of F-actin OOP (A), projected nuclear area (B) and nuclear eccentricity (C). Specifically, as F-actin OOP (A) and nuclear eccentricity (C) increased, T_{bx} decreased while K_{Tx} increased. However, as projected nuclear area increased, T_{bx} increased while K_{Tx} decreased. The correlation coefficient, r, is determined by linear regression analysis. Reported p values for Pearson correlations are two-tailed, demonstrated that the correlation is significantly different from zero. All plots: mean ± SEM. n = 13–18 cells per condition.

Discussion

In this study, we showed that VSMC shape can regulate its contractile function. We found that whereas wider width cells generate a greater force when stimulated with ET-1, longer, thinner VSMCs have a greater range of contraction relative to their basal tone. This suggests that where the vasculature requires a higher fidelity in its modulation of blood flow, longer, thinner cells are functionally advantageous. This is particularly relevant to vascular tissue engineering where there is a requirement that vascular grafts are compatible both anatomically and functionally at the graft site.[44] In the past two decades, several strategies have been explored to recapitulate the 3D architectural organization in native vessels.[45] Customarily these strategies rely on seeded cells to migrate and self-assemble into tissues with minimal guidance. While arterial replacements can be engineered *in vitro*, when engrafted, the compliance mismatch between the graft and native vessel results in thrombosis and intimal hyperplasia at the anastomotic site, resulting in low patency rate.[46] Our findings suggest that, in addition to closely matching the biomechanical aspects of healthy artery, engineering vascular grafts with VSMC shapes that mimic cellular architecture of the native, healthy vasculatures could improve functionality and long-term patency.

We previously reported that engineered VSM with forced elongated spindle shapes exerted greater contractile tensile stress when chemically stimulated.[47] The results reported herein are consistent with the findings by Tolic-Norrelykke and Wang, where they found that cells with wider width contracted with greater force than slimmer cells with a similar projected area.[26d] The differences in observed shape-contractility relationship between the current findings and our previous study by Alford and colleagues may be attributed to differences in measured quantities, experimental techniques and cellular micro-environmental conditions. Our previous study utilised the muscular thin film technology,[48] which measured the contractile strength of the VSM tissue with the component of Cauchy stress along the cell orientation. This measured quantity represented contractile force per tissue cross-sectional area, whereas the current study quantified the contractility of VSMCs *via* TFM, which measured the contractile force and strain energy exerted by the cell on the substrate. In addition, the engineered VSM tissue tested in Alford *et al.* was cultured with a higher level of cell–cell contact, the possibility of off axis alignment of cells, and stiffer abiotic substrates as compared to this single cell study. These differences in micro-environmental conditions will influence VSMC phenotype[49] and functions.[50] As a result, measured contractile strength may be reduced as it reflects an average of all cells in the tissue, including weakly or non-contractile cells and cells oriented in off-axis compared to the global orientation of the tissue.

Mechanical forces exerted on the exterior of a cell are propagated into the cell *via* the cellular cytoskeleton to the nuclear lamina,[35,51] directly affecting nuclear shape and gene transcription. While cell shape induced nucleus elongation has been well documented, the relative contribution between longitudinal tension and lateral compression imposed by the stress fibres on the nucleus is unknown.[52] Our finding that nuclear eccentricity negatively correlated with longitudinal traction force suggests that lateral compression forces exerted by stress fibres physically deforms the nucleus. This observation agrees with a recent report detailing how lateral compressive forces exerted on the nucleus are responsible for shape deformation, chromatin remodelling and reduced cell proliferation.[38] Others have proposed that compressive physical forces exerted by aligned actin fibres are required to expose transcription binding sites or DNA regulatory motifs, potentiating differences in DNA-associated protein binding and gene transcription.[53] Since nuclear shape deformation is correlated with physiological[26a,38,54] and pathological[55] changes in cellular functions, nuclear deformation may be indicative of, and further distinguish, the function and phenotype of vascular smooth muscle.

In this study, we demonstrated that isolated VSMCs with elongated shape exhibited less contractile strength but greater relative contractile increase upon stimulation. This shape-dependent contractile behaviour suggests that the elongated shape of VSMC in muscular arteries may lead to improved dynamic contractile range, a key feature required for effective vascular tone modulation *in vivo*. In addition to providing mechanical insight into the physiological structure–function relationship of VSMCs, our finding is particularly important for obtaining the desired VSMC contractile function from a clinical perspective in the design of a functionally active tissue engineered graft.[56] Our data suggest that providing organizational guidance cues to guide the development and assembly of VSMC into elongated shape may be beneficial in a successful implantation of a small artery graft.

Materials and methods

Sample preparation

Photolithography. Photolithographic chromium mask for microcontact printing were designed in AutoCAD (Autodesk Inc.) and fabricated at the Center for Nanoscale Systems facility with Heidelberg DWL-66 mask writer. The design for traction force microscopy (TFM) studies, consisted of rectangles of approximately 4000 μm^2 surface area and variable length to width ratios (5 : 1, 141 $\mu m \times 28 \mu m$; 10 : 1, 200 $\mu m \times 20 \mu m$; 20 : 1, 280 $\mu m \times 14 \mu m$). Silicon wafers (Wafer World) spin-coated with SU-8 2002 negative photoresist (MicroChem Corp.) were exposed to ultra-violet (UV) light to cross-link the designed pattern. Uncross-linked regions were dissolved by submerging the wafers in propylene glycol methyl ether acetate.

Microcontact printing of polyacrylamide gels. ECM protein FN after biotinylation modification was microcontact printed onto the polyacrylamide (PAA) substrate, as previous published.[4] Briefly, FN was cross-linked with biotin using Sulfo-NHS-LC-Biotin (Pierce). 13 kPa PAA gel substrate was fabricated with 5/0.1% acrylamide/bis concentration. Immediately prior to gel polymerization, streptavidin-acrylamide and 200 nm

fluorescent beads were added to the gel solution for a final concentration of 1 : 5 and 1 : 100, respectively, by volume. 15 μL of gel-bead solution was cured on activated 25 mm coverslips. 200 μg mL^{-1} biotinylated fibronectin (biotin-FN) was incubated on a PDMS (Sylgard 184, Dow Corning, Midland, MI) stamp with microscaled raised features for 1 h at room temperature and blown dry gently. The biotin-FN coated PDMS stamp was placed in contact with cured PAA gel, transferring the biotin-FN pattern to the substrate. The patterned PAA gel was stored in phosphate buffered saline (PBS) until cell seeding. When seeded, cells were constrained to the ECM patterned portion of the substrate after serum starvation.

Human umbilical artery smooth muscle cell culture

Human umbilical artery smooth muscle cells (Lonza, Walkersville, MD) purchased at passage 3 was cultured in growth medium consisted of M199 culture medium (GIBCO, Invitrogen, Carlsbad, CA) supplemented with 10% fetal bovine serum (FBS, Invitrogen), 10 mM HEPES (GIBCO, Invitrogen, Carlsbad, CA), 3.5 g L^{-1} glucose, 2 mg L^{-1} vitamin B-12, 50 U mL^{-1} penicillin and 50 U mL^{-1} streptomycin (GIBCO). All experiments were performed at passage 6–7.

VSMCs were seeded in growth media at 5000 cells cm^{-2} and allowed to attach to the isotropically patterned FN on PAA gel or patterned biotin-FN islands on PAA gel for 24 hours before replaced with a growth factor free medium consisted of M199, 10 mM HEPES, 3.5 g L^{-1} glucose, 2 mg L^{-1} vitamin B-12, 50 U mL^{-1} penicillin and 50 U mL^{-1} streptomycin to induce a contractile phenotype for 48 hours prior to cell staining or TFM experiments.

Fluorescent and immunohistochemical staining

VSMCs seeded on PAA gel after 3 d of culture were fixed with 4% formaldehyde solution (Thermo Scientific Pierce) for 10 minutes prior to staining. VSMCs seeded on isotropically patterned FN were stained for cell membrane (DiO, Invitrogen) and nucleus (DAPI) while VSMCs seeded on patterned biotin-FN islands were stained for F-actin (phalloidin, Molecular Probes) and nucleus (DAPI). Patterned FN islands were stained with rabbit anti-human fibronectin antibody (1 : 100 dilution, Sigma-Aldrich, St. Louis, MO) followed by Alexa Fluor 647 conjugated anti-rabbit secondary antibody (1 : 100 dilution, Abcam). The stained samples were then mounted with ProLong Gold antifade agent (Molecular Probes) and stored in −20 °C freezer until imaging.

Cell, patterned FN island, F-actin and nucleus fluorescent microscopy

Fixed and stained cells seeded on isotropically patterned FN were imaged on a line-scanning Zeiss LSM 5 LIVE confocal microscope (Carl Zeiss, Oberkochen, GER) with a 20× Plan-Apochromat objective at 1× zoom and laser excitations at 405 nm and 488 nm wavelengths to image the DAPI and DiO staining respectively. With the same microscope, stained micropatterned FN islands on PAA gel were imaged with a 20× Plan-Apochromat objective at 0.5× zoom and laser excitation at 633 nm wavelength. 2D and Z-stack images of phalloidin stained F-actin and DAPI stained nucleus were acquired with the Zeiss LSM 5 LIVE confocal microscopy with a 40× EC-Plan Neofluar lens oil objective with 1× zoom and laser excitations at 561 nm and 405 nm wavelength respectively. Z-stack images were subsequently deconvolved in Imaris (Bitplane Scientific Software).

Cell, F-actin, and nucleus image analysis

The spreading area of single cells on isotropically patterned FN was manually traced in ImageJ (rsbweb.nih.gov/ij/) and quantified. Cell AR was calculated by manually tracing the phalloidin stain in ImageJ. F-actin OOP was calculated from phalloidin stain with a coherence threshold of 0.3 using a structure tensor method.[30] Similar to a previous report by our group,[26a] cell thickness was calculated from deconvolved Z-stack images of F-actin, which closely approximated the actual cell thickness in engineered cardiomyocytes.[57] Nuclear angle offset (θ) was calculated by manually tracing the outlines of nucleus and cell body in ImageJ and comparing orientation difference between the principle axes. Nuclear eccentricity was evaluated by fitting an ellipse to individually traced nucleus in ImageJ and calculating its eccentricity, defined as:

$$e = \sqrt{1 - \left(\frac{\text{minor axis length}}{\text{major axis length}}\right)^2} \quad (1)$$

Projected nuclear area was quantified by tracing the outline of the nucleus in ImageJ. Nuclear volume (V) and surface area (SA) were evaluated by fitting an ellipsoid with half-length (a), half-width (b) and half-height (c) to each individual nucleus from deconvolved Z-stack images in Imaris (Fig. S2B, ESI†) with the following formulas:

$$V = \pi\tfrac{4}{3}abc \quad (2)$$

$$\text{SA} \approx 4\pi\left(\frac{a^p b^p + a^p c^p + b^p c^p}{3}\right)^{1/p} \quad (3)$$

where p = 1.6075. Cell shortening was calculated by summing the differences in cell length from DIC images of cell at basal and relaxed conditions (Fig. S5A, ESI†). OOP, nuclear angle offset, eccentricity, projected area, surface area, and volume were quantified from between 7–12 images of isolated VSMCs for each AR. All results were compared using ANOVA on ranks test, with pairwise comparisons performed using the Tukey's test. All correlations analysis was evaluated using Pearson product moment analysis.

Traction force microscopy

After 3 d of culture, micropatterned VSMCs on PAA gels were moved to an incubation chamber on a Zeiss LSM 5 LIVE confocal microscope maintained at 37 °C and immersed in Tyrode's solution (1.8 mM $CaCl_2$, 5 mM HEPES, 1 mM $MgCl_2$, 5.4 mM KCl, 135 mM NaCl, 0.33 mM NaH_2PO_4, adjusted to pH 7.4). After allowing the cells to equilibrate for 10 minutes in the incubation chamber, isolated VSMCs were imaged with a 40× EC Plan-Neofluar oil objective at 0.5× zoom on a Zeiss LSM 5 LIVE confocal microscope (Carl Zeiss, Oberkochen, GER) at

4-minute intervals 3 times with both bright field and 488 nm wavelength laser excitation to obtain images of VSMCs and displacing fluorescent beads in the gel substrate. Subsequently, the VSMCs were imaged at 4-minute intervals 3 times after stimulation with 100 nM ET-1 for 15 minutes, followed by 100 μM HA-1077 (Sigma-Aldrich, St. Louis, MO) for 15 minutes. During the stimulation, no images were taken to minimize the amount of photo-damage to cells. Immediately prior to cell detachment, cell nuclei were stained with DAPI and imaged to ensure that only single cells were analysed. At last, trypsin was added to detach the cells from the substrate. The experiment was terminated when the cell in the field of view dissociated from the gel, thus leaving the gel with no surface traction.

Traction force microscopy data analysis

Displacement and traction stress vectors were calculated from the bead displacement as previously published.[40] Briefly, displacement of gel was determined by comparing the beads images at baseline, stimulated and relaxed states to the bead image when cells were detached from the substrate. The traction stress field was then calculated from the displacement map using Fourier transform traction cytometry method. Traction stress vectors were discretised to a 10×10 μm^2 grid.

To calculate the total strain energy U transferred from the cell to the elastic distortion of the substrate, we applied the following equation as previously published:[27]

$$U = \frac{1}{2}\sum_n A_n\left(u_{x,n}T_{x,n} + u_{y,n}T_{y,n}\right) \quad (4)$$

where u_i and T_i represent displacement and traction force vectors in the i-direction; A is the discretised unit surface area of the cell body.

To calculate the total traction force cell T_i applied to the substrate in the i-direction, we summing the magnitudes of all traction force vectors $\vec{T}_{i,n}$ cell exerted on both sides and multiply by one half as previously published:[32]

$$T_i = \frac{1}{2}\sum_n A_n\left|\vec{T}_{i,n}\right| \quad (5)$$

assuming that cells exerted about equal magnitude of traction force on each side.

Isolated VSMC AR was calculated in ImageJ by tracing the cell outline from a DIC image taken at baseline. VSMCs that responded to ET-1 stimulation with significantly elevated strain energy were selected for correlation analysis. All correlation analysis was evaluated using Pearson product moment analysis.

Abbreviations

AR	Aspect ratio
DIC	Differential interference contrast
ET-1	Endothelin-1
FN	Fibronectin
OOP	Orientational order parameter
TFM	Traction force microscopy
VSMC	Vascular smooth muscle cells

Acknowledgements

The authors would like to thank Dr Megan L. McCain, Dr Leila F. Deravi and Mr Borna Dabiri for their comments on the manuscript. The authors gratefully acknowledge the use of facilities at the Harvard Center for Nanoscale Systems and the Wyss Institute for Biologically Inspired Engineering. This work was partially funded by the Defence Advanced Research Projects Agency cooperative agreement (W911NF-12-2-0036 for K.K.P.) and the School of Engineering and Applied Sciences, Harvard University.

References

1 J. A. Rhodin, Architecture of the vessel wall, *Comprehensive Physiology*, 2011.
2 P. F. Dillon, M. O. Aksoy, S. P. Driska and R. A. Murphy, Myosin phosphorylation and the cross-bridge cycle in arterial smooth muscle, *Science*, 1981, **211**, 495–497.
3 D. F. Bohr and R. Webb, Vascular smooth muscle function and its changes in hypertension, *Am. J. Med.*, 1984, **77**, 3.
4 (*a*) P. F. Davies, Flow-mediated endothelial mechanotransduction, *Physiol. Rev*, 1995, **75**, 519; (*b*) J. M. Tarbell, S. Weinbaum and R. D. Kamm, Cellular fluid mechanics and mechanotransduction, *Ann. Biomed. Eng.*, 2005, **33**, 1719–1723.
5 M. J. Davis and M. A. Hill, Signaling mechanisms underlying the vascular myogenic response, *Physiol. Rev*, 1999, **79**, 387–423.
6 V. Domenga, P. Fardoux, P. Lacombe, M. Monet, J. Maciazek, L. T. Krebs, B. Klonjkowski, E. Berrou, M. Mericskay and Z. Li, Notch3 is required for arterial identity and maturation of vascular smooth muscle cells, *Genes Dev.*, 2004, **18**, 2730–2735.
7 M. M. Ruchoux, D. Guerouaou, B. Vandenhaute, J.-P. Pruvo, P. Vermersch and D. Leys, Systemic vascular smooth muscle cell impairment in cerebral autosomal dominant arteriopathy with subcortical infarcts and leukoencephalopathy, *Acta Neuropathol.*, 1995, **89**, 500–512.
8 S. Rensen, P. Doevendans and G. Van Eys, Regulation and characteristics of vascular smooth muscle cell phenotypic diversity, *Neth. Heart J.*, 2007, **15**, 100–108.
9 E. C. Crouch, K. R. Stenmark and N. F. Voelkel, Smooth muscle-mediated connective tissue remodeling in pulmonary hypertension, *Am. J. Med. Genet*, 1986, **23**, 445.
10 P. Libby and H. Tanaka, The molecular bases of restenosis, *Prog. Cardiovasc. Dis.*, 1997, **40**, 97–106.
11 M. Yamaguchi-Okada, S. Nishizawa, M. Koide and Y. Nonaka, Biomechanical and phenotypic changes in the vasospastic canine basilar artery after subarachnoid hemorrhage, *J. Appl. Physiol.*, 2005, **99**, 2045–2052.

12 (*a*) A. Orekhov, I. Karpova, V. Tertov, S. Rudchenko, E. Andreeva, A. Krushinsky and V. Smirnov, Cellular composition of atherosclerotic and uninvolved human aortic subendothelial intima. Light-microscopic study of dissociated aortic cells, *Am. J. Pathol.*, 1984, **115**, 17; (*b*) A. Orekhov, E. Andreeva, A. Krushinsky, I. Novikov, V. Tertov, G. Nestaiko, K. A. Khashimov, V. Repin and V. Smirnov, Intimal cells and atherosclerosism, Relationship between the number of intimal cells and major manifestations of atherosclerosis in the human aorta, *Am. J. Pathol.*, 1986, **125**, 402; (*c*) A. N. Orekhov, A. V. Krushinsky, E. R. Andreeva, V. S. Repin and V. N. Smirnov, Adult human aortic cells in primary culture: heterogeneity in shape, *Heart Vessels*, 1986, **2**, 193–201.

13 L. R. Bonin, K. Madden, K. Shera, J. Ihle, C. Matthews, S. Aziz, N. Perez-Reyes, J. K. McDougall and S. C. Conroy, Generation and characterization of human smooth muscle cell lines derived from atherosclerotic plaque, *Arterioscler., Thromb., Vasc. Biol.*, 1999, **19**, 575–587.

14 J. Martínez-González, M. Berrozpe, O. Varela and L. Badimon, Heterogeneity of smooth muscle cells in advanced human atherosclerotic plaques: intimal smooth muscle cells expressing a fibroblast surface protein are highly activated by platelet-released products, *Eur. J. Clin. Invest.*, 2001, **31**, 939–949.

15 I. Konishi, S. Fujii, H. Okamura and T. Mori, Development of smooth muscle in the human fetal uterus: an ultrastructural study, *J. Anat.*, 1984, **139**, 239.

16 R. J. Kurman and H. J. Norris, Mesenchymal tumors of the uterus VI. Epithelioid smooth muscle tumors including leiomyoblastoma and clear-cell leiomyoma. A clinical and pathologic analysis of 26 cases, *Cancer*, 1976, **37**, 1853–1865.

17 F. J. Manasek, M. B. Burnside and R. E. Waterman, Myocardial cell shape change as a mechanism of embryonic heart looping, *Dev. Biol.*, 1972, **29**, 349–371.

18 P. W. Alford and L. A. Taber, Computational study of growth and remodelling in the aortic arch, *Comput. Methods Biomech. Biomed. Eng.*, 2008, **11**, 525–538.

19 (*a*) A. M. Gerdes, Cardiac myocyte remodeling in hypertrophy and progression to failure, *J. Card. Failure*, 2002, **8**, S264–S268; (*b*) A. M. Gerdes and J. M. Capasso, Structural remodeling and mechanical dysfunction of cardiac myocytes in heart failure, *J. Mol. Cell. Cardiol.*, 1995, **27**, 849–856; (*c*) A. M. Gerdes, S. E. Kellerman, J. A. Moore, K. E. Muffly, L. C. Clark, P. Y. Reaves, K. B. Malec, P. P. McKeown and D. D. Schocken, Structural remodeling of cardiac myocytes in patients with ischemic cardiomyopathy, *Circulation*, 1992, **86**, 426–430.

20 (*a*) Z. A. McCrossan, R. Billeter and E. White, Transmural changes in size, contractile and electrical properties of SHR left ventricular myocytes during compensated hypertrophy, *Cardiovasc. Res.*, 2004, **63**, 283–292; (*b*) K.-i. Sawada and K. Kawamura, Architecture of myocardial cells in human cardiac ventricles with concentric and eccentric hypertrophy as demonstrated by quantitative scanning electron microscopy, *Heart Vessels*, 1991, **6**, 129–142.

21 P.-L. Kuo, H. Lee, M.-A. Bray, N. A. Geisse, Y.-T. Huang, W. J. Adams, S. P. Sheehy and K. K. Parker, Myocyte Shape Regulates Lateral Registry of Sarcomeres and Contractility, *Am. J. Pathol.*, 2012, **181**, 2030–2037.

22 (*a*) A. W. Feinberg, P. W. Alford, H. Jin, C. M. Ripplinger, A. A. Werdich, S. P. Sheehy, A. Grosberg and K. K. Parker, Controlling the contractile strength of engineered cardiac muscle by hierarchal tissue architecture, *Biomaterials*, 2012, **33**, 5732–5741; (*b*) A. Grosberg, P.-L. Kuo, C.-L. Guo, N. A. Geisse, M.-A. Bray, W. J. Adams, S. P. Sheehy and K. K. Parker, Self-organization of muscle cell structure and function, *PLoS Comput. Biol.*, 2011, **7**, e1001088; (*c*) K. K. Parker, J. Tan, C. S. Chen and L. Tung, Myofibrillar architecture in engineered cardiac myocytes, *Circ. Res.*, 2008, **103**, 340–342.

23 S. R. Peyton and A. J. Putnam, Extracellular matrix rigidity governs smooth muscle cell motility in a biphasic fashion, *J. Cell. Physiol.*, 2005, **204**, 198–209.

24 (*a*) E. Stringa, V. Knauper, G. Murphy and J. Gavrilovic, Collagen degradation and platelet-derived growth factor stimulate the migration of vascular smooth muscle cells, *J. Cell Sci.*, 2000, **113**, 2055–2064; (*b*) R. A. Deaton, C. Su, T. G. Valencia and S. R. Grant, Transforming growth factor-beta1-induced expression of smooth muscle marker genes involves activation of PKN and p38 MAPK, *J. Biol. Chem.*, 2005, **280**, 31172–31181, DOI: 10.1074/jbc.M504774200.

25 (*a*) H. Qin, T. Ishiwata, R. Wang, M. Kudo, M. Yokoyama, Z. Naito and G. Asano, Effects of extracellular matrix on phenotype modulation and MAPK transduction of rat aortic smooth muscle cells *in vitro*, *Exp. Mol. Pathol.*, 2000, **69**, 79–90, DOI: 10.1006/exmp.2000.2321; (*b*) J. Thyberg and A. Hultgårdh-Nilsson, Fibronectin and the basement membrane components laminin and collagen type IV influence the phenotypic properties of subcultured rat aortic smooth muscle cells differently, *J. Cell Tissue Res.*, 1994, **276**, 263–271; (*c*) U. Hedin, B. A. Bottger, E. Forsberg, S. Johansson and J. Thyberg, Diverse effects of fibronectin and laminin on phenotypic properties of cultured arterial smooth muscle cells, *J. Cell Biol.*, 1988, **107**, 307–319.

26 (*a*) P. W. Alford, A. P. Nesmith, J. N. Seywerd, A. Grosberg and K. K. Parker, Vascular smooth muscle contractility depends on cell shape, *Integr. Biol.*, 2011, **3**, 1063–1070; (*b*) R. G. Thakar, Q. Cheng, S. Patel, J. Chu, M. Nasir, D. Liepmann, K. Komvopoulos and S. Li, Cell-shape regulation of smooth muscle cell proliferation, *Biophys. J.*, 2009, **96**, 3423–3432; (*c*) C. Williams, X. Q. Brown, E. Bartolak-Suki, H. Ma, A. Chilkoti and J. Y. Wong, The use of micropatterning to control smooth muscle myosin heavy chain expression and limit the response to transforming growth factor β1 in vascular smooth muscle cells, *Biomaterials*, 2011, **32**, 410–418; (*d*) I. M. Tolic-Norrelykke and N. Wang, Traction in smooth muscle cells varies with cell spreading, *J. Biomech.*, 2005, **38**, 1405–1412.

27 M. L. McCain, H. Lee, Y. Aratyn-Schaus, A. G. Kléber and K. K. Parker, Cooperative coupling of cell-matrix and cell–cell adhesions in cardiac muscle, *Proc. Natl. Acad. Sci. U. S. A.*, 2012, **109**, 9881–9886.

28 (*a*) R. L. Steward Jr, C.-M. Cheng, D. L. Wang and P. R. LeDuc, Probing cell structure responses through a shear and stretching mechanical stimulation technique, *Cell Biochem. Biophys.*, 2010, **56**, 115–124; (*b*) E. K. Yim, R. M. Reano, S. W. Pang, A. F. Yee, C. S. Chen and K. W. Leong, Nanopattern-induced changes in morphology and motility of smooth muscle cells, *Biomaterials*, 2005, **26**, 5405–5413.

29 R. Rezakhaniha, A. Agianniotis, J. T. C. Schrauwen, A. Griffa, D. Sage, C. Bouten, F. van de Vosse, M. Unser and N. Stergiopulos, Experimental investigation of collagen waviness and orientation in the arterial adventitia using confocal laser scanning microscopy, *Biomech. Model. Mechanobiol.*, 2012, **11**, 461–473.

30 D. Volfson, S. Cookson, J. Hasty and L. S. Tsimring, Biomechanical ordering of dense cell populations, *Proc. Natl. Acad. Sci. U. S. A.*, 2008, **105**, 15346–15351.

31 P. J. Steinhardt, D. R. Nelson and M. Ronchetti, Bond-orientational order in liquids and glasses, *Phys. Rev. B: Condens. Matter Mater. Phys.*, 1983, **28**, 784.

32 M. L. McCain, S. P. Sheehy, A. Grosberg, J. A. Goss and K. K. Parker, Recapitulating maladaptive, multiscale remodeling of failing myocardium on a chip, *Proc. Natl. Acad. Sci. U. S. A.*, 2013, **110**, 9770–9775.

33 K. Balachandran, P. W. Alford, J. Wylie-Sears, J. A. Goss, A. Grosberg, J. Bischoff, E. Aikawa, R. A. Levine and K. K. Parker, Cyclic strain induces dual-mode endothelial-mesenchymal transformation of the cardiac valve, *Proc. Natl. Acad. Sci. U. S. A.*, 2011, **108**, 19943–19948.

34 J. C. Nawroth, H. Lee, A. W. Feinberg, C. M. Ripplinger, M. L. McCain, A. Grosberg, J. O. Dabiri and K. K. Parker, A tissue-engineered jellyfish with biomimetic propulsion, *Nat. Biotechnol.*, 2012, **30**, 792–797.

35 A. J. Maniotis, C. S. Chen and D. E. Ingber, Demonstration of mechanical connections between integrins, cytoskeletal filaments, and nucleoplasm that stabilize nuclear structure, *Proc. Natl. Acad. Sci. U. S. A.*, 1997, **94**, 849–854.

36 J. R. Sims, S. Karp and D. E. Ingber, Altering the cellular mechanical force balance results in integrated changes in cell, cytoskeletal and nuclear shape, *J. Cell Sci.*, 1992, **103**, 1215–1222.

37 K. N. Dahl, A. J. Ribeiro and J. Lammerding, Nuclear shape, mechanics, and mechanotransduction, *Circ. Res.*, 2008, **102**, 1307–1318.

38 M. Versaevel, T. Grevesse and S. Gabriele, Spatial coordination between cell and nuclear shape within micropatterned endothelial cells, *Nat. Commun.*, 2012, **3**, 671.

39 L. Sherwood, *Human physiology: from cells to systems*, Thomson Brooks/Cole, 2012.

40 J. P. Butler, I. M. Tolić-Nørrelykke, B. Fabry and J. J. Fredberg, Traction fields, moments, and strain energy that cells exert on their surroundings, *Am. J. Physiol.: Cell Physiol.*, 2002, **282**, C595–C605.

41 T. Omelchenko, J. Vasiliev, I. Gelfand, H. Feder and E. Bonder, Mechanisms of polarization of the shape of fibroblasts and epitheliocytes: separation of the roles of microtubules and Rho-dependent actin–myosin contractility, *Proc. Natl. Acad. Sci. U. S. A.*, 2002, **99**, 10452–10457.

42 R. C. Webb, Smooth muscle contraction and relaxation, *Adv. Physiol. Educ.*, 2003, **27**, 201–206.

43 M.-A. P. Bray, W. J. Adams, N. A. Geisse, A. W. Feinberg, S. P. Sheehy and K. K. Parker, Nuclear morphology and deformation in engineered cardiac myocytes and tissues, *Biomaterials*, 2010, **31**, 5143–5150.

44 (*a*) D. G. Seifu, A. Purnama, K. Mequanint and D. Mantovani, Small-diameter vascular tissue engineering, *Nat. Rev. Cardiol.*, 2013, **10**, 410–421; (*b*) Y. Naito, T. Shinoka, D. Duncan, N. Hibino, D. Solomon, M. Cleary, A. Rathore, C. Fein, S. Church and C. Breuer, Vascular tissue engineering: towards the next generation vascular grafts, *Adv. Drug Delivery Rev.*, 2011, **63**, 312–323; (*c*) V. A. Kumar, L. P. Brewster, J. M. Caves and E. L. Chaikof, Tissue engineering of blood vessels: functional requirements, progress, and future challenges, *Cardiovasc. Eng. Technol.*, 2011, **2**, 137–148.

45 M. Peck, D. Gebhart, N. Dusserre, T. N. McAllister and N. L'Heureux, The evolution of vascular tissue engineering and current state of the art, *Cells Tissues Organs*, 2011, **195**, 144–158.

46 (*a*) R. Y. Kannan, H. J. Salacinski, P. E. Butler, G. Hamilton and A. M. Seifalian, Current status of prosthetic bypass grafts: a review, *J. Biomed. Mater. Res., Part B*, 2005, **74**, 570–581; (*b*) J. E. McBane, S. Sharifpoor, R. S. Labow, M. Ruel, E. J. Suuronen and J. Paul Santerre, Tissue engineering a small diameter vessel substitute: engineering constructs with select biomaterials and cells, *Curr. Vasc. Pharmacol.*, 2012, **10**, 347–360.

47 P. W. Alford, B. E. Dabiri, J. A. Goss, M. A. Hemphill, M. D. Brigham and K. K. Parker, Blast-induced phenotypic switching in cerebral vasospasm, *Proc. Natl. Acad. Sci. U. S. A.*, 2011, **108**, 12705–12710.

48 (*a*) M. Böl, S. Reese, K. K. Parker and E. Kuhl, Computational modeling of muscular thin films for cardiac repair, *Comput. Mech.*, 2009, **43**, 535–544; (*b*) P. W. Alford, A. W. Feinberg, S. P. Sheehy and K. K. Parker, Biohybrid thin films for measuring contractility in engineered cardiovascular muscle, *Biomaterials*, 2010, **31**, 3613–3621; (*c*) A. W. Feinberg, A. Feigel, S. S. Shevkoplyas, S. Sheehy, G. M. Whitesides and K. K. Parker, Muscular thin films for building actuators and powering devices, *Science*, 2007, **317**, 1366–1370.

49 S. R. Peyton, P. D. Kim, C. M. Ghajar, D. Seliktar and A. J. Putnam, The effects of matrix stiffness and RhoA on the phenotypic plasticity of smooth muscle cells in a 3-D biosynthetic hydrogel system, *Biomaterials*, 2008, **29**, 2597–2607.

50 (*a*) E. B. Uglow, S. Slater, G. B. Sala-Newby, C. M. Aguilera-Garcia, G. D. Angelini, A. C. Newby and S. J. George, Dismantling of cadherin-mediated cell-cell contacts modulates smooth muscle cell proliferation, *Circ. Res.*, 2003, **92**, 1314–1321; (*b*) X. Q. Brown, E. Bartolak-Suki, C. Williams, M. L. Walker, V. M. Weaver and J. Y. Wong, Effect of substrate stiffness and PDGF on the behavior of vascular smooth muscle cells: implications for atherosclerosis, *J. Cell. Physiol.*, 2010, **225**, 115–122; (*c*) E. Koutsouki,

C. Aguilera-Garcia, G. Sala-Newby, A. Newby and S. George, Cell-cell contact by cadherins provides an essential survival signal to migrating smooth muscle cells, *Eur. Heart J.*, 2003, **24**, 1838; (*d*) E. Koutsouki, C. A. Beeching, S. C. Slater, O. W. Blaschuk, G. B. Sala-Newby and S. J. George, N-Cadherin–Dependent Cell–Cell Contacts Promote Human Saphenous Vein Smooth Muscle Cell Survival, *Arterioscler., Thromb., Vasc. Biol.*, 2005, **25**, 982–988; (*e*) M. Jones, P. J. Sabatini, F. S. Lee, M. P. Bendeck and B. L. Langille, N-cadherin upregulation and function in response of smooth muscle cells to arterial injury, *Arterioscler., Thromb., Vasc. Biol.*, 2002, **22**, 1972–1977; (*f*) B. C. Isenberg, P. A. DiMilla, M. Walker, S. Kim and J. Y. Wong, Vascular smooth muscle cell durotaxis depends on substrate stiffness gradient strength, *Biophys. J.*, 2009, **97**, 1313–1322.

51 R. Bagby, Organization of contractile/cytoskeletal elements, *Biochem. Smooth Muscle*, 1983, **1**, 1–84.

52 K.-H. Kuo and C. Y. Seow, Contractile filament architecture and force transmission in swine airway smooth muscle, *J. Cell Sci.*, 2004, **117**, 1503–1511.

53 W. F. Liu, Mechanical regulation of cellular phenotype: implications for vascular tissue regeneration, *Cardiovasc. Res.*, 2012, **95**, 215–222.

54 (*a*) C. H. Thomas, J. H. Collier, C. S. Sfeir and K. E. Healy, Engineering gene expression and protein synthesis by modulation of nuclear shape, *Proc. Natl. Acad. Sci. U. S. A.*, 2002, **99**, 1972–1977; (*b*) S. A. Lelièvre, V. M. Weaver, J. A. Nickerson, C. A. Larabell, A. Bhaumik, O. W. Petersen and M. J. Bissell, Tissue phenotype depends on reciprocal interactions between the extracellular matrix and the structural organization of the nucleus, *Proc. Natl. Acad. Sci. U. S. A.*, 1998, **95**, 14711–14716; (*c*) F. Guilak, Compression-induced changes in the shape and volume of the chondrocyte nucleus, *J. Biomech.*, 1995, **28**, 1529–1541.

55 (*a*) D. Zink, A. H. Fischer and J. A. Nickerson, Nuclear structure in cancer cells, *Nat. Rev. Cancer*, 2004, **4**, 677–687; (*b*) B. C. Capell and F. S. Collins, Human laminopathies: nuclei gone genetically awry, *Nat. Rev. Genet.*, 2006, **7**, 940–952; (*c*) M. Webster, K. L. Witkin and O. Cohen-Fix, Sizing up the nucleus: nuclear shape, size and nuclear-envelope assembly, *J. Cell Sci.*, 2009, **122**, 1477–1486; (*d*) K.-H. Chow, R. E. Factor and K. S. Ullman, The nuclear envelope environment and its cancer connections, *Nat. Rev. Cancer*, 2012, **12**, 196–209.

56 M. S. Conte, The ideal small arterial substitute: a search for the Holy Grail?, *FASEB J.*, 1998, **12**, 43–45.

57 N. A. Geisse, S. P. Sheehy and K. K. Parker, Control of myocyte remodeling *in vitro* with engineered substrates, *In Vitro Cell. Dev. Biol.: Anim.*, 2009, **45**, 343–350.